THE JOURNAL OF PHYSICAL CHEMISTRY B

Article

pubs.acs.org/JPCB

Infrared and Raman Spectroscopy from Ab Initio Molecular Dynamics and Static Normal Mode Analysis: The C−H Region of DMSO as a Case Study

Sean A. Fischer,[†] Tyler W. Ueltschi,[‡] Patrick Z. El-Khoury,[*,§] Amanda L. Mifflin,[‡] Wayne P. Hess,[§] Hong-Fei Wang,[†] Christopher J. Cramer,[∥] and Niranjan Govind[*,†]

[†]William R. Wiley Environmental Molecular Sciences Laboratory, Pacific Northwest National Laboratory, P.O. Box 999, Richland, Washington 99352, United States

[‡]Department of Chemistry, University of Puget Sound, 1500 North Warner Street, Tacoma, Washington 98416, United States

[§]Physical Sciences Division, Pacific Northwest National Laboratory, P.O. Box 999, Richland, Washington 99352, United States

[∥]Department of Chemistry, Supercomputing Institute and Chemical Theory Center, University of Minnesota, 207 Pleasant Street South East, Minneapolis, Minnesota 55455, United States

Supporting Information

ABSTRACT: Carbon−hydrogen (C−H) vibration modes serve as key probes in the chemical identification of hydrocarbons and in vibrational sum-frequency generation spectroscopy of hydrocarbons at the liquid/gas interface. Their assignments pose a challenge from a theoretical viewpoint. In this work, we present a detailed study of the C−H stretching region of dimethyl sulfoxide using a new ab initio molecular dynamics (AIMD) module that we have implemented in NWChem. Through a combination of AIMD simulations and static normal mode analysis, we interpret experimental infrared and Raman spectra and explore the role of anharmonic effects in this system. Comprehensive anharmonic normal mode analysis of the C−H stretching region casts doubt upon previous experimental assignments of the shoulder on the symmetric C−H stretching peak. In addition, our AIMD simulations also show significant broadening of the in-phase symmetric C−H stretching resonance, which suggests that the experimentally observed shoulder is due to thermal broadening of the symmetric stretching resonance.

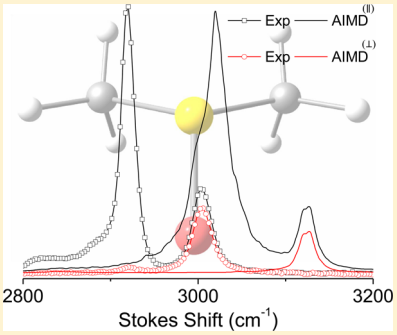

INTRODUCTION

Carbon−hydrogen (C−H) stretching vibrations are sensitive markers of the local chemical environment. Such vibrations are typically strongly infrared or Raman-active and are isolated in the 3000 ± 200 cm^{-1} spectral region. These are among the features that render C−H vibrations popular, for instance, in nonlinear vibrational spectroscopic and microscopic tools aimed at rapid imaging of biological systems.[1−3] C−H vibrations have also been predominantly used as probes in vibrational sum-frequency generation (SFG) spectroscopy to study hydrocarbons at liquid/gas interfaces.[4−6] Nonetheless, establishing a direct link between spectroscopic observables and theoretical predictions has proven to be a challenging task. This is a result of the inherent complexity of the high-energy vibrational band profiles, consisting of overlapping fundamental vibrational modes, overtones, combination modes, and Fermi resonances. Overall, capturing all of the aforementioned features is necessary for a faithful reproduction of experimentally recorded vibrational line shapes and comprises a real challenge from a theoretical viewpoint.

The standard approach of empirically scaling vibrational spectra computed based on the quantum mechanical harmonic oscillator approximation[7−9] is often inadequate, particularly when C−H stretching modes are targeted.[10−13] In this regard, several approaches have been proposed to go beyond the harmonic approximation. These include the vibrational self-consistent field (VSCF) approach,[10,14−17] methods based on perturbative corrections to the harmonic approximation,[18,19] and approaches based on ab initio molecular dynamics (AIMD) simulations.[20−29] AIMD simulations are particularly appealing in that they allow conformational sampling in phase space while treating the electronic structure of the molecular system within the Born−Oppenheimer approximation (i.e., the dynamics are propagated on an adiabatic potential energy surface). This becomes particularly important for molecules with internal rotations that create multiple thermally accessible minima on the potential energy surface. The traditional calculation of normal mode-dependent dipole and polarizability derivatives to simulate infrared and Raman spectra in the static approach or frequency domain is replaced by Fourier transforms of the dipole and polarizability correlation functions in the time

Special Issue: Bruce C. Garrett Festschrift

Received: April 6, 2015
Revised: July 28, 2015
Published: July 29, 2015

DOI: 10.1021/acs.jpcb.5b03323
J. Phys. Chem. B 2016, 120, 1429−1436

domain dynamics simulations.[26] Because no approximations are invoked to approximate the shape of the potential energy landscape in AIMD simulations, vibrational spectra evaluated from these simulations are inherently more physical than their harmonic analogues that are evaluated at a minimum.[30] In principle, with adequate statistical sampling and in the absence of significant mode coupling leading to combination bands and Fermi resonances, the only assumptions stem from the level of the underlying electronic structure approach used to treat the molecular system.[31,32]

In this work, we present computational results obtained using a new module that we have implemented in the NWChem computational chemistry program[33] to perform Born−Oppenheimer molecular dynamics (BOMD) simulations using Gaussian basis functions to represent the electronic structure. Using a combination of AIMD simulations and static normal mode analysis (NMA), we carefully analyze the C−H stretching region of a prototypical molecular system, namely, dimethyl sulfoxide (DMSO). DMSO was chosen as a test case because it is a relatively simple system that does not show complicated Fermi resonances like those seen in methanol, ethanol, and other hydrocarbons. Additionally, new spectroscopic techniques such as high-resolution broadband SFG spectroscopy[5] have the spectral resolving power to identify overlapping peaks, which offer more stringent tests of computational predictions.[6,34,35] Our results demonstrate the advantages of combining the two theoretical approaches to analyze and interpret experimental IR and Raman spectra. In the remainder of the paper we outline the methodology of computing IR/Raman spectra from AIMD simulations, provide details of the computational parameters and experimental setup, and discuss the insights into the C−H stretching vibrations that were gained.

COMPUTATIONAL DETAILS

The absorption line shape $I(\omega)$ for infrared absorption and the differential Raman scattering cross sections $\lambda_s^{-4}((d^2\sigma)/(d\omega d\Omega))$ can be related to Fourier transforms of autocorrelation functions of molecular properties[36]

$$I(\omega) = \frac{1}{2\pi}\int_{-\infty}^{\infty} \mathrm{d}t\, \exp^{-i\omega t}\langle \boldsymbol{\mu}(0)\cdot\boldsymbol{\mu}(t)\rangle \tag{1}$$

where I is the intensity, ω is the frequency, and $\boldsymbol{\mu}$ is the molecular electric dipole moment

$$\lambda_s^4\left(\frac{d^2\sigma}{d\omega d\Omega}\right)_{\parallel} = \frac{1}{2\pi}\int_{-\infty}^{\infty} \mathrm{d}t\, \exp^{-i\omega t}\frac{1}{15}\sum_{i,j}\langle \alpha_{ii}(0)\alpha_{jj}(t) + 2\alpha_{ij}(0)\alpha_{ij}(t)\rangle$$
$$= \frac{1}{2\pi}\int_{-\infty}^{\infty} \mathrm{d}t\, \exp^{-i\omega t}\frac{1}{15}\langle 15\bar{\alpha}(0)\bar{\alpha}(t) + 2\mathrm{Tr}\boldsymbol{\beta}(0)\cdot\boldsymbol{\beta}(t)\rangle \tag{2}$$

$$\lambda_s^4\left(\frac{d^2\sigma}{d\omega d\Omega}\right)_{\perp} = \frac{1}{2\pi}\int_{-\infty}^{\infty} \mathrm{d}t\, \exp^{-i\omega t}\frac{1}{30}\sum_{i,j}\langle 3\alpha_{ij}(0)\alpha_{ij}(t) - \alpha_{ii}(0)\alpha_{jj}(t)\rangle$$
$$= \frac{1}{2\pi}\int_{-\infty}^{\infty} \mathrm{d}t\, \exp^{-i\omega t}\frac{1}{10}\langle \mathrm{Tr}\boldsymbol{\beta}(0)\cdot\boldsymbol{\beta}(t)\rangle \tag{3}$$

where $2\pi\lambda_s$ is the wavelength of the scattered radiation, σ is the scattering cross section, Ω is a solid angle, $\bar{\alpha} = 1/3\mathbf{Tr}\boldsymbol{\alpha}$ is the isotropic part of the molecular polarizability tensor, and $\boldsymbol{\beta} = \boldsymbol{\alpha} - \bar{\alpha}\mathbf{I}$ is the anisotropic part and $\mathbf{I}$ is a unit tensor. The angle brackets refer to an ensemble average. Equation 2 corresponds to radiation scattered parallel to the polarization of the incident light and eq 3 corresponds to radiation scattered perpendicular to the polarization of the incident light.

To calculate the relevant correlation functions, we have performed AIMD simulations of an isolated DMSO molecule within the canonical ensemble. We have found for DMSO that performing calculations in the canonical ensemble rather than the microcanonical ensemble leads to better agreement with experimental spectra. (See the Supporting Information.) Because we are using classical correlation functions instead of their quantum analogues, we apply the harmonic approximation quantum correction, Q_{HA}

$$Q_{\mathrm{HA}} = \frac{\hbar\omega}{k_{\mathrm{B}}T\left(1 - \exp\left[-\frac{\hbar\omega}{k_{\mathrm{B}}T}\right]\right)} \tag{4}$$

where $\hbar$ is the reduced Planck constant, k_{B} is the Boltzmann constant, and T is the temperature of the simulation. The quantum line shape and scattering cross sections are obtained by multiplying the classical values by Q_{HA}. Ramírez et al. found that this correction was the only one to obey the fluctuation−dissipation theorem and comprises the best approximation in most cases.[37]

To perform the molecular dynamics simulations, we have implemented a new module into NWChem that is capable of performing BOMD using Gaussian basis functions with various thermostats and at any level of theory in NWChem where gradients of the electronic energy are available, including excited-state molecular dynamics using linear-response time-dependent density functional theory (LR-TDDFT).[38] The velocity-Verlet algorithm was used[39] to propagate nuclei. For temperature control, we have implemented the stochastic velocity-rescaling thermostat of Bussi, Donadio, and Parrinello,[40] which correctly samples the canonical ensemble (under the assumption of ergodicity) and minimally impacts dynamic properties. The electronic structure was calculated with the B3LYP[41−43] exchange-correlation functional in conjunction with the 6-311++G**[44,45] basis set. This functional and basis set combination was used in a previous study of the Raman spectrum of DMSO and found to give reliable agreement with experiment.[46]

Following the suggestions of Horníček et al.,[31] we performed several short trajectories, which were averaged together to obtain the final result. The geometry of DMSO was initially optimized on the electronic ground state without enforcing symmetry. We then initiated a ∼5 ps trajectory starting from the minimized structure. The system was propagated at 300 K, and 20 structures were randomly extracted and used as initial structures for our production runs. Initial velocities were assigned from a 300 K Maxwell−Boltzmann distribution with center of mass translation and rotation removed. We integrated each of the 20 trajectories for 430 000 au with a time step of 10 au (∼0.2419 fs) for a total simulation time of over 200 ps. Note that for the length of trajectory that we utilized, our spectral resolution is ∼3.5 cm^{-1}. In the Supporting Information we have also calculated an IR spectrum using only the first half of each trajectory to verify that our results are converged with respect to trajectory length. Frequency-dependent molecular polarizability tensors for Raman analysis were computed at every step in each of the trajectories in the velocity gauge using the response module of NWChem[47−52] at an incident wavelength of 800 nm to match with the excitation wavelength used in the experiments outlined later. Prior to analysis, all quantities were

DOI: 10.1021/acs.jpcb.5b03323
J. Phys. Chem. B 2016, 120, 1429−1436

rotated to a common frame-of-reference to remove any spurious rotations that may have occurred during the AIMD simulations. The first 3000 steps of each trajectory were discarded in the calculation of the correlation functions and spectra. Fast Fourier transforms (FFTs) were used to calculate the correlation functions, and an exponential or Poisson window function[53] was applied to the correlation functions before another FFT was performed to obtain the spectra according to eqs 1−3. We chose a parameter for the window function such that the resulting Lorentzian line shapes feature a full width at half-maximum of 10 cm^{-1}.

To complement our AIMD analysis, we have also performed harmonic and anharmonic normal-mode analyses. A static NMA, including IR intensities and Raman activities, was performed using Gaussian 09[54] with the same basis set and functional. The frequencies predicted by the standard NMA are often qualitatively correct yet lack quantitative accuracy due to the anharmonicity of the potential energy surfaces. As mentioned in the Introduction, one commonly adopted approach to correct the harmonic frequencies is to apply empirical scaling factors, either individually to different Hessian matrix elements or a single value to all harmonic frequencies, to align the computed spectra with their experimental analogues;[55] however, merely scaling the frequencies to match experiment offers no deeper insight into the molecular vibrations and can mask deficiencies in the underlying theory. A more rigorous approach is to directly account for anharmonicities through perturbation theory. This also allows for the calculation of overtones, combination bands, and Fermi resonances, quantities that are absent in the harmonic NMA and the AIMD-based simulations. In the present work we computed anharmonic corrections to the harmonic frequencies and IR intensities using second-order perturbation (VPT2) with numerical third and fourth derivatives,[18] as implemented in Gaussian 09. We applied the same width parameter used to broaden the MD spectra to broaden the computed static spectra.

EXPERIMENTAL METHODS

The high-resolution femtosecond stimulated Raman (HR-FSRS) spectrometer used to record simulated Raman loss (SRL) spectra is described in detail elsewhere.[6] The system is based on an amplified ∼90 ps Raman pump synchronized with a ∼40 fs laser source used to generate white light continuum. The fundamentals of the femtosecond and picosecond sources are centered at ∼800 nm and operated at a repetition rate of 1 kHz. The picosecond pump source (50 mW) and femtosecond white light continuum are focused into a quartz cell (1 cm path length) containing a spectroscopic-grade liquid DMSO sample. SRL of the pump is recorded using a 500 mm spectrograph and a charge-coupled device camera by the consecutive ratio of on/off modes of the long 800 nm pulse. The combination of a 500 mm spectrograph and a 1200 mm^{-1} grating amounts to an effective spectral resolution of ∼1.5 cm^{-1}. The gas-phase infrared absorption spectrum was taken from the NIST chemistry WebBook.[56]

RESULTS AND DISCUSSION

Before examining the Raman spectra, we first validated our AIMD approach against the experimental gas-phase and static normal-mode IR spectra of DMSO. Vibrations in DMSO have been previously assigned based on a combination of experimental IR and Raman spectroscopy and normal coordinate analyses.[57,58] These previous works also considered deuterated DMSO; however, in the present study we concern ourselves only with nondeuterated isotopologue DMSO. Our normal coordinate analysis is in agreement with the assignment of the lower frequency feature in the C−H stretching region to the symmetric C−H stretch and the higher frequency feature assignment to the degenerate stretch. Table 1 gives the harmonic and anharmonic frequencies from the NMA, along with the mode assignments and irreducible representations of the modes. We use the same labeling conventions as Horrocks and Cotton.[57] From this static analysis we can see that the degenerate stretch feature is composed of four fundamental transitions, while the symmetric stretch feature is composed of two fundamentals. Figure 1 shows the IR spectrum computed analytically from the harmonic NMA at the ground-state minimum and that obtained from the MD simulations. These are compared with the experimental gas-phase IR spectrum taken from the NIST database.[56] Both simulated spectra overestimate the frequencies of the features as well as the spacing between features, which is not unexpected. After the VPT2 correction to the NMA spectrum, there is significantly better agreement with the experimental spectrum. While the

Table 1. Irreducible Representations, Mode Assignments, and Unscaled Harmonic Frequencies Based on the Static Normal Mode Analysis (NMA) and Anharmonic Frequencies from VPT2[a]

mode	NMA	VPT2
degenerate stretches		
$A'\ \nu_1$	3148.2	2999.1
$A''\ \nu_{14}$	3147.1	2998.4
$A'\ \nu_2$	3139.1	2991.1
$A''\ \nu_{15}$	3135.2	2987.8
symmetric stretches		
$A'\ \nu_3$	3040.2	2924.0
$A''\ \nu_{16}$	3037.9	2921.1

[a]All frequencies are given in wave numbers (cm^{-1}). The labeling follows that of Horrocks and Cotton.[57]

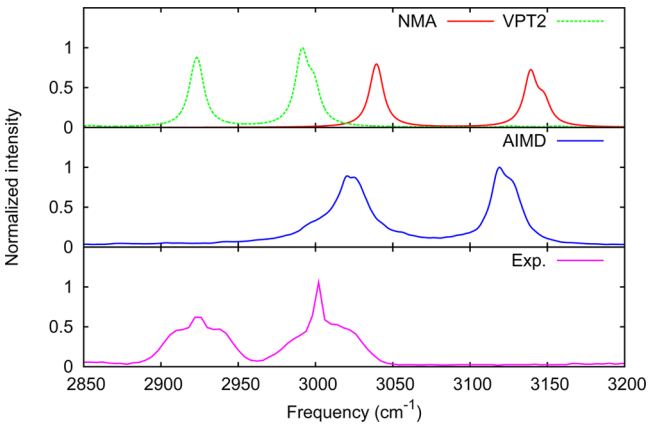

Figure 1. Infrared absorption spectra the standard normal-mode analysis (top row) at both the harmonic frequencies (NMA) and anharmonic frequencies (VPT2), MD simulation using eqs 1 and 4 (middle row), and experimental gas-phase measurement[56] (bottom row). The simulated spectra have been artificially broadened by 10 cm^{-1}.

DOI: 10.1021/acs.jpcb.5b03323
J. Phys. Chem. B 2016, 120, 1429−1436

AIMD approach inherently captures the anharmonicity of the potential energy surface, the anharmonic shift that is obtained is proportional to the amplitude of the vibration. Because of the use of classical mechanics for the nuclear dynamics in the AIMD simulation, the energy available to the C−H stretching modes at the simulation temperature of 300 K is significantly below the quantum zero-point energy of the modes. This is the origin of the small shift from the harmonic values seen in the AIMD IR spectrum. Some recent work has looked at attempting to capture certain nuclear quantum effects while still performing classical dynamics.[59−61] The limited exploration of the potential means the AIMD results have to be looked upon with caution; however, given that the anharmonic IR intensities calculated with VPT2 are so similar to the harmonic ones, we feel confident that for this system the main effect of the limited exploration of the potential will be overestimated frequencies. The simulated spectra predict very similar envelopes for the degenerate stretching feature, while the AIMD simulation naturally predicts a broader peak for the symmetric stretching feature. Overall, all simulated results are in reasonable agreement with the experimental measurement.

Turning to the Raman spectra shown in Figure 2, the comparisons between simulated and measured Raman spectra

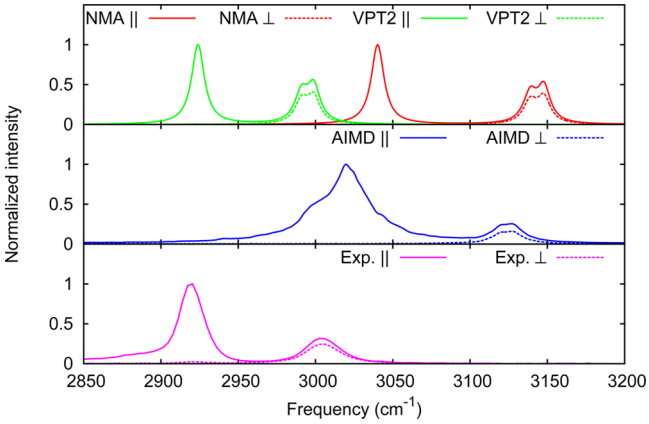

Figure 2. Raman scattering spectra from the normal-mode analysis (top) at both the harmonic frequencies (NMA) and anharmonic frequencies (VPT2); from AIMD simulation using eqs 2, 3, and 4 (middle); and from the HR-FSRS experiment previously described (bottom). The simulated spectra have been artificially artificially broadended by 10 cm^{-1}.

are similar to those observed for the IR spectra. We note that while the experimental Raman spectra were obtained in the liquid phase and the simulations were on an isolated DMSO molecule, previous work on methanol and ethanol found that the experimental gas-phase and liquid-phase Raman spectra were very similar.[62,63] AIMD and harmonic static frequencies are blue-shifted relative to the experimental spectra, and the spacing between symmetric and degenerate stretching modes is again overestimated. Better agreement is obtained when the intensities of the harmonic spectra are shifted to the anharmonic frequencies, although the intensity of the degenerate stretching peak is overestimated. While Raman intensities are known to be very sensitive to the basis set employed,[64] previous work[65] found that the 6-311++G** basis set, the one employed in the current study, had an average percent normalized root-mean-square deviation of 4.3% when compared with the results obtained with larger basis sets. Both simulation methods give good depolarization ratios for the degenerate stretch, and the AIMD result is in good agreement with the relative intensities of the experimental symmetric stretching and degenerate stretching features.

The experimental Raman spectra present two features that merit further scrutiny. The shoulder and tail on the low-frequency side of the parallel orientation symmetric stretch feature (which begins to rise at ∼2880 cm^{-1}) have been previously assigned to either an overtone of the CH_3 deformation modes that occur in the 1400−1450 cm^{-1} region[66,67] or as a Fermi resonance between the deformation mode overtone and the C−H symmetric stretch.[5] There is also a small feature in the perpendicular spectrum that occurs at the same frequency as the symmetric stretch; however, as a symmetric mode, this vibrational resonance should be strongly polarized. The same feature is also observed, albeit without comment, in the work of Forel and Tranquille.[58] Because neither theoretical prediction includes this small depolarized feature, we are hindered in our ability to comment on it; however, its absence does suggest that the feature possibly arises as a result of intermolecular interactions, which are not accounted for in our present simulations. Further work is warranted to address that issue. In the ensuing analysis, we will focus our discussion on the origin of the shoulder in the symmetric stretching feature.

The anharmonic frequency calculation does not predict a Fermi resonance between the symmetric C−H stretching and an overtone of the CH_3 deformation modes. Additionally, the overtones of the deformation modes are predicted to occur between 2583 and 2855 cm^{-1}. While we cannot readily rule out the shoulder as an overtone, the 66 cm^{-1} gap between the highest frequency deformation mode overtone and the lowest frequency symmetric stretching mode makes the assignment of this spectral signature to an overtone somewhat questionable. Additionally, an overtone is generally expected to have a much smaller intensity than the fundamental transition. Using the anharmonic IR intensities calculated by VPT2 as a guide because we do not have access to anharmonic Raman intensities, the difference in intensity of an overtone is at least an order of magnitude smaller than the fundamental. If this holds for the Raman intensities, the intensity of a deformation overtone relative to the symmetric stretching fundamental would be approximately 2 orders of magnitude smaller. Experimentally, the intensity of the shoulder is 10% that of the symmetric stretch. We have verified the results of our static calculations by performing the same calculations with MP2/6-311++G** (NMA and VPT2) and CCSD/6-311++G** (NMA). Those results can be found in the Supporting Information. In the parallel Raman spectrum calculated from the AIMD simulations, there is a clear asymmetry in the symmetric stretch features. It should be noted that while the AIMD simulation is inherently anharmonic because no assumptions are made about the shape of the potential, certain anharmonic effects, such as combination bands and Fermi resonances, are not captured because the nuclear motion is treated classically.[30−32] To address the origin of the shoulder observed in the parallel spectrum, we calculated the vibrational density of states from the Fourier transform of the autocorrelation function of the mass-weighted atomic velocities.[30] For additional detail, we separated the contributions by element. As expected, carbon and hydrogen are the only elements that contribute to the C−H stretching region (Figure 3).

DOI: 10.1021/acs.jpcb.5b03323
J. Phys. Chem. B 2016, 120, 1429−1436

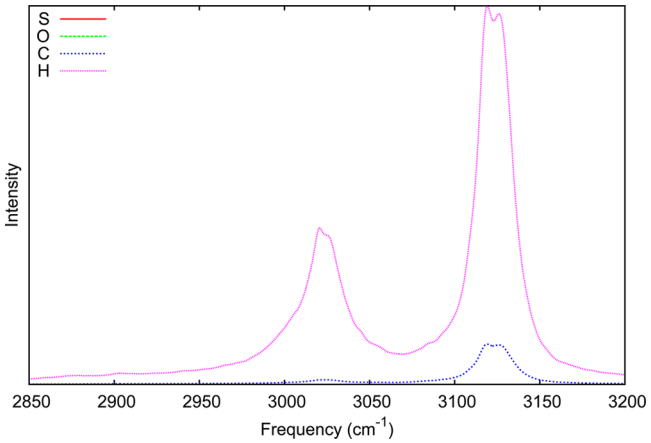

Figure 3. Element-wise decomposition of the vibrational density of states calculated from the Fourier transform of the momentum autocorrelation function.

On the basis of the NMA, only the in-phase, symmetric C−H stretch contributes to the symmetric stretch feature in the Raman spectra. To ascertain the contribution of the two symmetric stretching modes to the AIMD spectra, we have computed the Fourier transforms of the autocorrelation functions of the symmetry coordinates for the in-phase and out-of-phase symmetric C−H stretching modes (ν_3 and ν_{16}, respectively). These are given in terms of the C−H bond lengths (r) as

$$S_3 = 6^{-1/2}(r_1 + r_2 + r_3 + r_4 + r_5 + r_6) \quad (5)$$

$$S_{16} = 6^{-1/2}(r_1 + r_2 + r_3 - r_4 - r_5 - r_6) \quad (6)$$

where r_1 through r_3 cover one methyl group and r_4 through r_6 cover the other methyl group. A full list of symmetry coordinates for DMSO can be found in the work of Horrocks and Cotton.[57]

We can see from Figure 4 that the in-phase mode, S_3, features the same envelope as the calculated Raman parallel spectrum, in agreement with the selection rules derived from the static calculations. This suggests that the shoulder on the Raman spectrum could be a finite temperature effect rather than an overtone or a Fermi resonance. Recall that for an

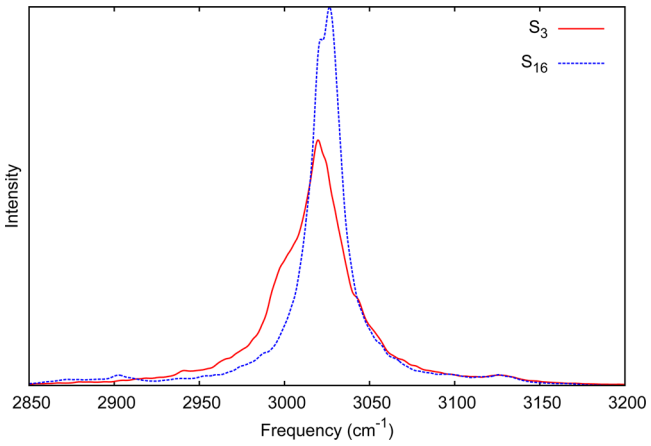

Figure 4. Fourier transform of the autocorrelation functions of the symmetry coordinates for the symmetric C−H stretching modes, eqs 5 and 6.

anharmonic potential the frequency is dependent on the amplitude of vibration. Except for an isolated diatomic molecule, there is no reason to assume that the amplitude of a vibration will remain constant over the course of a molecular trajectory. If there is any anharmonicity in the potential, then variations in the amplitude of a vibration would lead to a distribution of frequencies and thus to vibrational line broadening. We note that it is implicitly assumed that each vibration has a fixed amplitude in the static calculations, which is why only a single frequency is calculated for each mode, even for the perturbative anharmonic correction. To further explore this effect, we calculated the energy of DMSO as the atoms were displaced along the in-phase and out-of-phase stretching modes.

Figure 5 clearly demonstrates that the in-phase mode, ν_3, has significant anharmonicity; in particular, there is a clear cubic

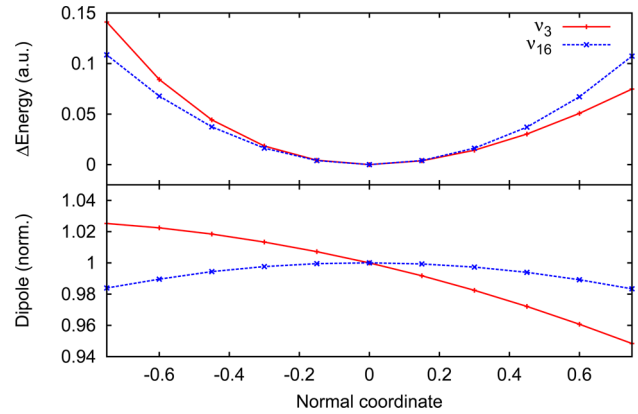

Figure 5. Energy in atomic units as a function of normal mode coordinates for the symmetric C−H stretching modes (top). The energy is referenced to that of the ground-state minimum. The in-phase mode (ν_3) potential shows a clear, significant cubic component, while the out-of-phase mode potential is far more symmetric. The bottom panel shows the corresponding dipole moment magnitudes. The dipoles have been normalized to the equilibrium value.

component to the potential. Because of the cubic nature of the potential, the dipole moment of DMSO is not symmetric about displacements along the in-phase normal mode (bottom panel Figure 5). This cubic contribution is important because it will give rise to an asymmetric line shape as different parts of the potential are explored. The standard practice of dressing the results of a static calculation with a Lorentzian or Gaussian function to mimic broadening completely misses this asymmetry in the line shape. These characteristics of the potential could explain the appearance of a shoulder on the low-frequency side of the symmetric stretching feature in the Raman spectrum. On the basis of the evidence from the anharmonic static calculations and the AIMD simulations, we propose that the observed shoulder on the symmetric stretching feature is due to thermal broadening of the in-phase symmetric stretching mode.

CONCLUSIONS

We have described and demonstrated a powerful new functionality of NWChem: Gaussian basis-set-based Born−Oppenheimer molecular dynamics. The molecular dynamics module leverages the scalability of NWChem to allow for large-scale molecular dynamics simulations. As a prototypical application, we have used this new module in concert with a

DOI: 10.1021/acs.jpcb.5b03323
J. Phys. Chem. B 2016, 120, 1429−1436

more conventional static NMA, to perform a somewhat detailed analysis of the C−H stretching region of the Raman spectra of DMSO. Our anharmonic NMA calls into question the previous experimental assignment of the shoulder on the symmetric C−H stretching peak as an overtone or Fermi resonance. No Fermi resonance between the C−H stretching modes and the CH_3 deformation modes is predicted, and the overtones of the deformation modes are at least 60 cm^{-1} away from the C−H stretching modes and expected to have an intensity far below what is seen in experiment. The AIMD simulations also show significant broadening of the in-phase symmetric C−H stretching resonance. This result is rationalized in terms of the strong cubic component of the in-phase symmetric stretching mode and the asymmetric dipole moment with displacements along this mode. Our findings therefore lead us to suggest that the shoulder is due to thermal broadening of the symmetric stretching resonance.

Our results highlight the advantage of combining traditional normal-mode analyses with AIMD-based vibrational spectra. The normal modes from the static calculations allow for more detailed interpretation of the AIMD results, while AIMD offers a detailed analysis of the role of anharmonicities predicted with the static calculations. In future work we will expand our simulations of vibrational spectroscopies to include SFG spectroscopy. The high-resolution and low signal-to-noise ratio of new SFG techniques[5,6,34,35] present the opportunity to test computational predicitions and would benefit greatly from the interpretive power of simulations.

■ ASSOCIATED CONTENT

Supporting Information

The Supporting Information is available free of charge on the ACS Publications website at DOI: 10.1021/acs.jpcb.5b03323.

Comparison of microcanonical and canonical ensemble results for the AIMD IR spectrum and MP2 and CCSD normal-mode analyses with VPT2 corrections for the MP2 results. (PDF)

■ AUTHOR INFORMATION

Corresponding Authors

*P.Z.E.: E-mail: patrick.elkhoury@pnnl.gov.
*N.G.: E-mail: niri.govind@pnnl.gov.

Notes

The authors declare no competing financial interest.

■ ACKNOWLEDGMENTS

This material is based on work supported by the U.S. Department of Energy (DOE), Office of Science, Office of Advanced Scientific Computing Research, Scientific Discovery through Advanced Computing (SciDAC) program under Award Numbers DE-SC0008666 (C.J.C.) and KC030102062653 (S.A.F, N.G.). P.Z.E. acknowledges support from the Laboratory Directed Research and Development Program through a Linus Pauling Fellowship at Pacific Northwest National Laboratory (PNNL) and an allocation of computing time from the National Science Foundation (TG-CHE130003). W.P.H. acknowledges support from the U.S. DOE, Office of Science, Office of Basic Energy Sciences, Division of Chemical Sciences, Geosciences & Biosciences under Award Number KC030102016248. T.W.U. and A.L.M. were supported in part by the U.S. DOE, Office of Science, Office of Workforce Development for Teachers and Scientists (WDTS) under the Visiting Faculty Program (VFP). This work also benefitted from resources provided by PNNL Institutional Computing. This research was performed using EMSL, a DOE Office of Science User Facility sponsored by the Office of Biological and Environmental Research and located at PNNL. PNNL is operated by Battelle Memorial Institute for the United States Department of Energy under DOE contract number DE-AC05-76RL1830.

■ REFERENCES

(1) Evans, C. L.; Potma, E. O.; Puoris'haag, M.; Cote, D.; Lin, C. P.; Xie, X. S. Chemical Imaging of Tissue *In Vivo* with Video-Rate Coherent Anti-Stokes Raman Scattering Microscopy. *Proc. Natl. Acad. Sci. U. S. A.* **2005**, *102*, 16807−16812.

(2) Freudiger, C. W.; Min, W.; Saar, B. G.; Lu, S.; Holtom, G. R.; He, C.; Tsai, J. C.; Kang, J. X.; Xie, X. S. Label-Free Biomedical Imaging with High Sensitivity by Stimulated Raman Scattering Microscopy. *Science* **2008**, *322*, 1857−1861.

(3) Chung, C.-Y.; Boik, J.; Potma, E. O. Biomolecular Imaging with Coherent Nonlinear Vibrational Microscopy. *Annu. Rev. Phys. Chem.* **2013**, *64*, 77−99.

(4) Lu, R.; Gan, W.; Wu, B. H.; Zhang, Z.; Guo, Y.; Wang, H.-F. C-H Stretching Vibrations of Methyl, Methylene and Methine Groups at the Vapor/Alcohol (n = 18) Interfaces. *J. Phys. Chem. B* **2005**, *109*, 14188−14129.

(5) Velarde, L.; Zhang, X.-Y.; Lu, Z.; Joly, A. G.; Wang, Z.; Wang, H.-F. Communication: Spectroscopic Phase and Lineshapes in High-Resolution Broadband Sum Frequency Vibrational Spectroscopy: Resolving Interfacial Inhomogeneities of Identical Molecular Groups. *J. Chem. Phys.* **2011**, *135*, 241102.

(6) Velarde, L.; Wang, H.-F. Unified Treatment and Measurement of the Spectral Resolution and Temporal Effects in Frequency-Resolved Sum-Frequency Generation Vibrational Spectroscopy (SFG-VS). *Phys. Chem. Chem. Phys.* **2013**, *15*, 19970−19984.

(7) Pulay, P.; Fogarasi, G.; Pang, F.; Boggs, J. E. Systematic *Ab Initio* Gradient Calculation of Molecular Geometries, Force Constants, and Dipole Moment Derivatives. *J. Am. Chem. Soc.* **1979**, *101*, 2550−2560.

(8) Irikura, K. K.; Johnson, R. D.; Kacker, R. N. Uncertainties in Scaling Factors for *Ab Initio* Vibrational Frequencies. *J. Phys. Chem. A* **2005**, *109*, 8430−8437.

(9) Alecu, I. M.; Zheng, J.; Zhao, Y.; Truhlar, D. G. Computational Thermochemistry: Scale Factor Databases and Scale Factors for Vibrational Frequencies Obtained from Electronic Model Chemistries. *J. Chem. Theory Comput.* **2010**, *6*, 2872−2887.

(10) Bowman, J. M. The Self-Consistent-Field Approach to Polyatomic Vibrations. *Acc. Chem. Res.* **1986**, *19*, 202−208.

(11) Brauer, B.; Gerber, R. B.; Kabeláč, M.; Hobza, P.; Bakker, J. M.; Abo Riziq, A. G.; de Vries, M. S. Vibrational Spectroscopy of the G···C Base Pair: Experiment, Harmonic and Anharmonic Calculations, and the Nature of the Anharmonic Couplings. *J. Phys. Chem. A* **2005**, *109*, 6974−6984.

(12) Chaban, G. M.; Jung, J. O.; Gerber, R. B. Anharmonic Vibrational Spectroscopy of Glycine: Testing of *Ab Initio* and Empirical Potentials. *J. Phys. Chem. A* **2000**, *104*, 10035−10044.

(13) Šebek, J.; Pele, L.; Potma, E. O.; Gerber, R. B. Raman Spectra of Long Chain Hydrocarbons: Anharmonic Calculations, Experiment and Implications for Imaging of Biomembranes. *Phys. Chem. Chem. Phys.* **2011**, *13*, 12724−12733.

(14) Gerber, R. B.; Chaban, G. M.; Brauer, B.; Miller, Y. *Theory and Applications of Computational Chemistry: The First 40 Years*; Elsevier: Amsterdam, 2005; Chapter 9, pp 165−193.

(15) Jung, J. O.; Gerber, R. B. Vibrational Wave Functions and Spectroscopy of $(H_2O)_n$, n = 2,3,4,5: Vibrational Self-Consistent Field with Correlation Corrections. *J. Chem. Phys.* **1996**, *105*, 10332−10348.

(16) Brauer, B.; Pincu, M.; Buch, V.; Bar, I.; Simons, J. P.; Gerber, R. B. Vibrational Spectra of Alpha-Glucose, Beta-Glucose, and Sucrose: Anharmonic Calculations and Experiment. *J. Phys. Chem. A* **2011**, *115*, 5859−5872.

DOI: 10.1021/acs.jpcb.5b03323
J. Phys. Chem. B 2016, 120, 1429−1436

(17) Christiansen, O. Vibrational Structure Theory: New Vibrational Wave Function Methods for the Calculation of Anharmonic Vibrational Energies and Vibrational Contributions to Molecular Properties. *Phys. Chem. Chem. Phys.* **2007**, *9*, 2942−2953.
(18) Barone, V. Anharmonic Vibrational Properties by a Fully Automated Second-Order Perturbative Approach. *J. Chem. Phys.* **2005**, *122*, 014108.
(19) Cappelli, C.; Monti, S.; Scalmani, G.; Barone, V. On the Calculation of Vibrational Frequencies for Molecules in Solution Beyond the Harmonic Approximation. *J. Chem. Theory Comput.* **2010**, *6*, 1660−1669.
(20) Thar, J.; Reckien, W.; Kirchner, B. In *Atomistic Approaches in Modern Biology: from Quantum Chemistry to Molecular Simulations*; Reiher, M., Ed.; Topics in Current Chemistry; Springer: Berlin, 2007; Vol. *268*, pp 133−171.
(21) Thar, J.; Brehm, M.; Seitsonen, A. P.; Kirchner, B. Unexpected Hydrogen Bond Dynamics in Imidazolium-Based Ionic Liquids. *J. Phys. Chem. B* **2009**, *113*, 15129−15132.
(22) Pensado, A. S.; Brehm, M.; Thar, J.; Seitsonen, A. P.; Kirchner, B. Effect of Dispersion on the Structure and Dynamics of the Ionic Liquid 1-Ethyl-3-Methylimidazolium Thiocyanate. *ChemPhysChem* **2012**, *13*, 1845−1853.
(23) Malberg, F.; Pensado, A. S.; Kirchner, B. The Bulk and the Gas Phase of 1-Ethyl-3-Methylimidazolium Ethylsulfate: Dispersion Interaction Makes the Difference. *Phys. Chem. Chem. Phys.* **2012**, *14*, 12079−12082.
(24) Bruessel, M.; Brehm, M.; Pensado, A. S.; Malberg, F.; Ramzan, M.; Stark, A.; Kirchner, B. On the Ideality of Binary Mixtures of Ionic Liquids. *Phys. Chem. Chem. Phys.* **2012**, *14*, 13204−13215.
(25) Brehm, M.; Weber, H.; Pensado, A. S.; Stark, A.; Kirchner, B. Proton Transfer and Polarity Changes in Ionic Liquid-Water Mixtures: A Perspective on Hydrogen Bonds from *Ab Initio* Molecular Dynamics at the Example of 1-Ethyl-3-Methylimidazolium Acetate-Water Mixtures-Part 1. *Phys. Chem. Chem. Phys.* **2012**, *14*, 5030−5044.
(26) Kirchner, B.; di Dio, P. J.; Hutter, J. In *Multiscale Molecular Methods In Applied Chemistry*; Kirchner, B., Vrabec, J., Eds.; Topics in Current Chemistry; Springer: Berlin, 2012; Vol. *307*, pp 109−153.
(27) Schmidt, J.; VandeVondele, J.; Kuo, I. F. W.; Sebastiani, D.; Siepmann, J. I.; Hutter, J.; Mundy, C. J. Isobaric-Isothermal Molecular Dynamics Simulations Utilizing Density Functional Theory: An Assessment of the Structure and Density of Water at Near-Ambient Conditions. *J. Phys. Chem. B* **2009**, *113*, 11959−11964.
(28) Marx, D. Proton Transfer 200 Years After von Grotthuss: Insights from *Ab Initio* Simulations. *ChemPhysChem* **2006**, *7*, 1848−1870.
(29) Car, R.; Parrinello, M. Unified Approach for Molecular-Dynamics and Density-Functional Theory. *Phys. Rev. Lett.* **1985**, *55*, 2471−2474.
(30) Thomas, M.; Brehm, M.; Fligg, R.; Vöhringer, P.; Kirchner, B. Computing Vibrational Spectra from *Ab Initio* Molecular Dynamics. *Phys. Chem. Chem. Phys.* **2013**, *15*, 6608−6622.
(31) Horníček, J.; Kaprálová, P.; Bouř, P. Simulations of Vibrational Spectra from Classical Trajectories: Calibration with *Ab Initio* Force Fields. *J. Chem. Phys.* **2007**, *127*, 084502.
(32) Hudecová, J.; Hopmann, K. H.; Bouř, P. Correction of Vibrational Broadening in Molecular Dynamics Clusters with the Normal Mode Optimization Method. *J. Phys. Chem. B* **2012**, *116*, 336−342.
(33) Valiev, M.; Bylaska, E. J.; Govind, N.; Kowalski, K.; Straatsma, T. P.; van Dam, H. J. J.; Wang, D.; Nieplocha, J.; Apra, E.; Windus, T. L.; et al. NWChem: A Comprehensive and Scalable Open-Source Solution for Large Scale Molecular Simulations. *Comput. Phys. Commun.* **2010**, *181*, 1477−1489.
(34) Wang, H.-F.; Velarde, L.; Gan, W.; Fu, L. Quantitative Sum-Frequency Generation Vibrational Spectroscopy of Molecular Surfaces and Interfaces: Lineshape, Polarization, and Orientation. *Annu. Rev. Phys. Chem.* **2015**, *66*, 189−216.
(35) Mifflin, A. L.; Velarde, L.; Ho, J.; Psciuk, B. T.; Negre, C. F. A.; Ebben, C. J.; Upshur, M. A.; Lu, Z.; Strick, B. L.; Thomson, R. J.; et al. Accurate Line Shapes from Sub-1 cm^{-1} Resolution Sum Frequency Generation Vibrational Spectroscopy of α-Pinene at Room Temperature. *J. Phys. Chem. A* **2015**, *119*, 1292−1302.
(36) McQuarrie, D. A. *Statistical Mechanics*; University Science Books: Sausalito, CA, 2000; Chapter 21.
(37) Ramírez, R.; López-Ciudad, T.; Kumar, P.; Marx, D. Quantum Corrections to Classical Time-Correlation Functions: Hydrogen Bonding and Anharmonic Floppy Modes. *J. Chem. Phys.* **2004**, *121*, 3973−3983.
(38) Silverstein, D. W.; Govind, N.; van Dam, H. J. J.; Jensen, L. Simulating One-Photon Absorption and Resonance Raman Scattering Spectra Using Analytical Excited State Gradients within Time-Dependent Density Functional Theory. *J. Chem. Theory Comput.* **2013**, *9*, 5490.
(39) Swope, W. C.; Andersen, H. C.; Berens, P. H.; Wilson, K. R. A Computer Simulation Method for the Calculation of Equilibrium Constants for the Formation of Physical Clusters of Molecules: Application to Small Water Clusters. *J. Chem. Phys.* **1982**, *76*, 637−649.
(40) Bussi, G.; Donadio, D.; Parrinello, M. Canonical Sampling Through Velocity Rescaling. *J. Chem. Phys.* **2007**, *126*, 014101.
(41) Becke, A. D. Density-Functional Thermochemistry 0.3. The Role of Exact Exchange. *J. Chem. Phys.* **1993**, *98*, 5648−5652.
(42) Lee, C. T.; Yang, W. T.; Parr, R. G. Development of the Colle-Salvetti Correlation-Energy Formula into a Functional of the Electron-Density. *Phys. Rev. B: Condens. Matter Mater. Phys.* **1988**, *37*, 785−789.
(43) Vosko, S. H.; Wilk, L.; Nusair, M. Accurate Spin-Dependent Electron Liquid Correlation Energies for Local Spin-Density Calculations - A Critical Analysis. *Can. J. Phys.* **1980**, *58*, 1200−1211.
(44) Krishnan, R.; Binkley, J. S.; Seeger, R.; Pople, J. A. Self-Consistent Molecular-Orbital Methods 0.20. Basis Set for Correlated Wave-Functions. *J. Chem. Phys.* **1980**, *72*, 650−654.
(45) McLean, A. D.; Chandler, G. S. Contracted Gaussian-Basis Sets for Molecular Calculations 0.1. 2nd Row Atoms, Z = 11−18. *J. Chem. Phys.* **1980**, *72*, 5639−5648.
(46) Singh, S.; Srivastava, S. K.; Singh, D. K. Raman Scattering and DFT Calculations Used for Analyzing the Structural Features of DMSO in Water and Methanol. *RSC Adv.* **2013**, *3*, 4381−4390.
(47) Krykunov, M.; Autschbach, J. Calculation of Optical Rotation with Time-Periodic Magnetic-Field-Dependent Basis Functions in Approximate Time-Dependent Density-Functional Theory. *J. Chem. Phys.* **2005**, *123*, 114103.
(48) Jensen, L.; Autschbach, J.; Schatz, G. C. Finite Lifetime Effects on the Polarizability within Time-Dependent Density-Functional Theory. *J. Chem. Phys.* **2005**, *122*, 224115.
(49) Krykunov, M.; Banerjee, A.; Ziegler, T.; Autschbach, J. Calculation of Verdet Constants with Time-Dependent Density Functional Theory: Implementation and Results for Small Molecules. *J. Chem. Phys.* **2005**, *122*, 074105.
(50) Autschbach, J. Computation of Optical Rotation Using Time-Dependent Density Functional Theory. *Comput. Lett.* **2007**, *3*, 131−150.
(51) Hammond, J. R.; Govind, N.; Kowalski, K.; Autschbach, J.; Xantheas, S. S. Accurate Dipole Polarizabilities for Water Cluster n = 2−12 at the Coupled-Cluster Level of Theory and Benchmarking of Various Density Functionals. *J. Chem. Phys.* **2009**, *131*, 214103.
(52) Aquino, F. W.; Schatz, G. C. Time-Dependent Density Functional Methods for Raman Spectra in Open-Shell Systems. *J. Phys. Chem. A* **2014**, *118*, 517−525.
(53) Harris, F. J. On the Use of Windows for Harmonic Analysis with the Discrete Fourier Transform. *Proc. IEEE* **1978**, *66*, 51−83.
(54) Frisch, M. J.; Trucks, G. W.; Schlegel, H. B.; Scuseria, G. E.; Robb, M. A.; Cheeseman, J. R.; Scalmani, G.; Barone, V.; Mennucci, B.; Petersson, G. A.; et al. *Gaussian 09*, revision C.01; Gaussian, Inc.: Wallingford, CT, 2010.
(55) Andersson, M. P.; Uvdal, P. New Scale Factors for Harmonic Vibrational Frequencies Using the B3LYP Density Functional Method with the Triple-ζ Basis Set 6-311+G(d,p). *J. Phys. Chem. A* **2005**, *109*, 2937−2941.

DOI: 10.1021/acs.jpcb.5b03323
J. Phys. Chem. B 2016, 120, 1429−1436

(56) Lias, S. G.; Bartmess, J. E.; Liebman, J. F.; Holmes, J. L.; Levin, R. D.; Mallard, W. G. In *NIST Chemistry WebBook, NIST Standard Reference Database Number 69*; Linstrom, P. J., Mallard, W. G., Eds.; National Institute of Standards and Technology: Gaithersburg, MD, 2005.
(57) Horrocks, W. D., Jr.; Cotton, F. A. Infrared and Raman Spectra and Normal Co-Ordinate Analysis of Dimethyl Sulfoxide and Dimethyl Sulfoxide-D6. *Spectrochim. Acta* **1961**, *17*, 134−147.
(58) Forel, M.-T.; Tranquille, M. Spectres de Vibration du Diméthylsulfoxyde et dn Diméthylsulfoxyde-D6. *Spectrochim. Acta, Part A* **1970**, *26*, 1023−1034.
(59) Van-Oanh, N.-T.; Falvo, C.; Calvo, F.; Lauvergnat, D.; Basire, M.; Gaigeot, M.-P.; Parneix, P. Improving Anharmonic Infrared Spectra Using Semiclassically Prepared Molecular Dynamics Simulations. *Phys. Chem. Chem. Phys.* **2012**, *14*, 2381−2390.
(60) Ceriotti, M.; Bussi, G.; Parrinello, M. Nuclear Quantum Effects in Solids Using a Colored-Noise Thermostat. *Phys. Rev. Lett.* **2009**, *103*, 030603.
(61) Ceriotti, M.; Bussi, G.; Parrinello, M. Colored-Noise Thermostats á la Carte. *J. Chem. Theory Comput.* **2010**, *6*, 1170−1180.
(62) Yu, Y.; Lin, K.; Zhou, X.; Wang, H.; Liu, S.; Ma, X. New C-H Stretching Vibrational Spectral Features in the Raman Spectra of Gaseous and Liquid Ethanol. *J. Phys. Chem. C* **2007**, *111*, 8971−8978.
(63) Yu, Y.; Wang, Y.; Lin, K.; Hu, N.; Zhou, X.; Liu, S. Complete Raman Spectral Assignment of Methanol in the C-H Stretching Region. *J. Phys. Chem. A* **2013**, *117*, 4377−4384.
(64) Halls, M. D.; Schlegel, H. B. Comparison Study of the Prediction of Raman Intensities Using Electronic Structure Methods. *J. Chem. Phys.* **1999**, *111*, 8819−8824.
(65) Cheeseman, J. R.; Frisch, M. J. Basis Set Dependence of Vibrational Raman and Raman Optical Activity. *J. Chem. Theory Comput.* **2011**, *7*, 3323−3334.
(66) Selvarajan, A. Raman Spectrum of Dimethyl Sulfoxide (DMSO) and the Influence of Solvents. *Proc. Indian Acad. Sci.* **1966**, *64*, 44−50.
(67) Allen, H. C.; Gragson, D. E.; Richmond, G. L. Molecular Structure and Adsorption of Dimethyl Sulfoxide at the Surface of Aqueous Solutions. *J. Phys. Chem. B* **1999**, *103*, 660−666.

DOI: 10.1021/acs.jpcb.5b03323
J. Phys. Chem. B 2016, 120, 1429−1436